Atmos. Chem. Phys. Discuss., 8, 21089–21128, 2008
www.atmos-chem-phys-discuss.net/8/21089/2008/

Atmospheric Chemistry and Physics Discussions

This discussion paper is/has been under review for the journal *Atmospheric Chemistry and Physics (ACP)*. Please refer to the corresponding final paper in *ACP* if available.

Ice supersaturations and cirrus cloud crystal numbers

M. Krämer[1], C. Schiller[1], A. Afchine[1], R. Bauer[1], I. Gensch[1], A. Mangold[1,*], S. Schlicht[1,], N. Spelten[1], N. Sitnikov[2], S. Borrmann[3], M. de Reus[3], and P. Spichtinger[4]**

[1]FZ Jülich, ICG-I, Germany
[2]CAO, Region Moscow, Russia
[3]Univ. Mainz, Inst. Phys. Atmos., Germany
[4]ETH Zürich, Inst. Atmos. andClimate, Switzerland
[*]now at: Royal Met. Inst. of Belgium, Brussels, Belgium
[**]now at: Mühlenbachstraße 5, 52134 Herzogenrath, Germany

Received: 20 October 2008 – Accepted: 20 October 2008 – Published: 17 December 2008

Correspondence to: M. Krämer (m.kraemer@fz-juelich.de)

Published by Copernicus Publications on behalf of the European Geosciences Union.

Abstract

Upper tropospheric observations outside and inside of cirrus clouds of water vapour mixing ratios sometimes exceeding water saturation, yielding up to more than 200% relative humidities over ice (RH_{ice}) have been reported from aircraft and balloon measurements in recent years. From these observations a lively continuous discussion arose on whether there is a lack of understanding of ice cloud microphysics or if the water measurements are tainted with large uncertainties or flaws.

Here, RH_{ice} in clear air and in ice clouds is investigated: strictly quality checked aircraft in-situ observations of RH_{ice} were performed during 28 flights in tropical, mid-latitude and Arctic field experiments in the temperature range 183–250 K. In our field measurements, no supersaturations above water saturation are found. Nevertheless, super- or subsaturations inside of cirrus are frequently observed at low temperatures (<205 K) in our field data set. To explain persistent RH_{ice} deviating from saturation, we analysed the number densities of ice crystals recorded during 20 flights. From the combined analysis – using conventional microphysics – of supersaturations and ice crystal numbers, we show that the high, persistent supersaturations observed inside of cirrus are caused by unexpected, frequent very low ice crystal numbers that could hardly be explained by homogeneous ice nucleation. Heterogeneous ice formation or the suppression of freezing might better explain the observed ice crystal numbers. Thus, our lack of understanding of the high supersaturations with implications to the microphysical and radiative properties of cirrus, the vertical redistribution of water and climate, is traced back to the understanding of the freezing process at low temperatures.

1 Introduction

The relative humidity over ice RH_{ice} controls the formation of cirrus clouds in the upper troposphere. Prior to ice formation, when an air parcel cools while rising, RH_{ice} increases up to the freezing threshold necessary to nucleate ice in the ambient aerosol

particles. Alfred Wegener was probably the first who recognized that atmospheric air can be supersaturated with respect to ice without forming ice crystals. During his second expedition to Greenland in 1911/1912 he recognized that moist breathing of his horses produced small ice crystals (Wall, 1942) growing in the ice supersaturated air. Gierens et al. (2000) and Spichtinger et al. (2003) recalled the work of Glückauf (1945) and Weickmann (1945), who already mentioned that cirrus clouds form not as soon as ice saturation is reached and that ice-forming regions in the upper troposphere are regions of high ice supersaturation that should occur frequently.

Today's state of knowledge is that the freezing thresholds depend on the compounds of the available ice forming aerosol particles. In case these particles are pure liquid solutions (of arbitrary composition), the – homogeneous – freezing thresholds range for 140...180% for T=240...180 K and are well described by the theory derived by Koop et al. (2000). In the presence of aerosol particles containing an insoluble impurity (so called ice nuclei, IN, such as soot, mineral dust or biological particles), the – heterogeneous – freezing thresholds are determined by the composition of the particles. Therefore, up to now no simple parametrisation scheme exists for the heterogeneous freezing thresholds. In most cases they are lower than the homogeneous freezing thresholds and can be significantly different. Thus, injection of aerosol particles with lower freezing threshold would directly impact to the cirrus cloud cover and thus the radiation balance of the atmosphere (Gettelman and Kinnison, 2007).

Once the ice cloud has formed, the gas phase water and thus RH_{ice} is depleted by the growing ice crystals in dependence on their number and size. The ice cloud microphysics interacts with in-cloud RH_{ice} (see e.g. Gensch et al., 2008) because it affects the water vapour condensation rate and fall speed of the ice crystals (Khvorostyanov et al., 2006) that in turn influences the vertical redistribution of water in the upper troposphere.

Forced by the recent insight in the importance of both, the clear sky and in-cloud RH_{ice}, for the Earth's climate, many airborne and remote sensing experiments as well as model studies were recently performed to investigate the distributions of RH_{ice} in the

upper troposphere (Kelly et al., 1993; Heymsfield and Milosevitch, 1995; Heymsfield et al., 1998; Gierens et al., 1999; Gierens et al., 2000; Jensen et al., 2001; Ovarlez et al., 2002; Haag et al., 2003; Spichtinger et al., 2003; Spichtinger et al., 2004; Gayet et al., 2004; Comstock and Ackerman, 2004; Lee et al., 2004; Gao et al., 2004; Jensen et al., 2005a; Jensen et al., 2005b; Gayet et al., 2006; Gettelman et al., 2006; MacKenzie et al., 2006; Popp et al., 2007; Vömel and David, 2007; Immler et al., 2008).

The major results of these studies are sorted into two temperature ranges (T<200 K and T=200–240 K) and are listed in Table 1. The warmer temperature range corresponds to cirrus at altitudes between about 6 and 15 km in Arctic, mid-latitude and tropical regions, while cirrus in the colder temperature range are found in the tropics between about 15 and 20 km. Since most aircraft can reach only the lower altitudes, the warmer cirrus clouds and their environment are more extensively investigated and thus already a quite consistent picture exists.

At higher temperatures (T>200 K), supersaturations up to the homogenous freezing threshold occur frequently under clear sky conditions as well as inside of cirrus clouds. Occasionally higher supersaturations were observed. At lower temperatures(T<200 K), where the H_2O concentrations are much lower so that the measurements become challenging for the water instruments, the observations become less frequent. In many of the aircraft and balloon studies RH_{ice} up to or even more than water saturation were reported outside and inside of the cold cirrus clouds.

As outlined earlier, we can understand supersaturations up to the freezing thresholds in both, clear air as well as inside cirrus. But, supersaturations up to water saturation or even above raise the question if these are caused by instrument artefacts or if “the basic principles underpinning the current understanding of ice cloud formation and alter the assessment of water distribution in the upper troposphere are called into question”, as Peter et al. (2006) summarised.

Another crucial point in the frame of this discussion is the existence of persistently high supersaturations inside of cirrus clouds. It is believed that the in-cloud initial high supersaturation is reduced to saturation very quickly – in the timescale of minutes –

by consumption of gas phase water by the numerous growing ice crystals formed by homogeneous freezing, which is believed to be the major process forming ice in the upper troposphere (Hoyle et al., 2005). However, Korolev and Mazin (2003) showed that one important parameter controlling the water vapour relaxation time and RH_{ice} is the product of the mean number and size of the ice crystals, $N_{ice} \cdot R_{ice}$, the so called integral ice crystal radius, which is inversely linked to RH_{ice}. Thus, in case of low $N_{ice} \cdot R_{ice}$, RH_{ice} could also become persistent.

Here, we present an extensive data set of strongly quality checked in-situ clear sky and in-cloud aircraft observations of RH_{ice} and N_{ice}, R_{ice} in the temperature range 183–250 K. The measurements are performed during 28 flights in the frame of ten field campaigns in the Arctic, at mid-latitudes and in the Tropics. Based on the comprehensive field data set, we examine the possible atmospheric range of supersaturations and relaxation times resulting from the observed cirrus microphysical parameters for the complete ice cloud temperature range. We further derive frequencies of occurrence of RH_{ice} in 1 K temperature bins and discuss the pattern of RH_{ice} found in clear air and inside of cirrus as well as those of N_{ice}, R_{ice}. Finally, we investigate the freezing mechanism consistent with the observed ice crystal numbers for warmer and colder cirrus. We show that there is strong indication that cold ice clouds (<205 K) contain a lower ice crystal number than expected.

2 Experimentals

Water vapour and ice crystal measurements from several instruments operated on three different research aircraft, i.e. the high-altitude Russian M55 Geophysika and the German research aircraft *enviscope*-Learjet and DLR Falcon, are analyzed in the present study. Only a brief description of each instrument is given here as greater detail is available in the referenced literature. The instruments and the parameters derived from their measurements are listed in Table 2, the campaigns and flights are listed in Table 3.

2.1 Water vapour

During field experiments with the M55 Geophysika, water vapour was determined simultaneously with the FISH and the FLASH, both closed cell Lyman-α fluorescence hygrometers (Zöger et al., 1999; Schiller et al., 2008; Sitnikov et al., 2007). The FISH is equipped with a forward facing inlet sampling H_2O_{enh}, i.e. gas phase+enhanced ice water. Ice particles are over-sampled with an enhancement ranging from 3 to 10 depending on the inlet's geometry, altitude and cruising speed of the aircraft. FLASH uses a downward facing inlet that excludes ice particles and samples only gas phase water, H_2O_{gas}. In experiments with the German *enviscope*-Learjet or DLR Falcon FISH is used for the H_2O_{enh} measurements, while H_2O_{gas} was measured with the open path TDL OJSTER (MayComm Instruments, May and Webster, 1993). The relative humidity with respect to ice, RH_{ice}, is calculated from H_2O_{gas} and the measurement of the ambient temperature, as listed in Table 2. The term "supersaturation" refers to relative humidities with respect to ice that exceeds 100%.

When in a cirrus cloud, H_2O_{enh} greatly exceeds H_2O_{gas} due to the additional water from the evaporated ice particles which are in addition sampled with an enhanced efficiency (see above). The H_2O_{enh} measurements with the FISH are important for two reasons: (i) we compare the FISH to the other H_2O_{gas} instrument in regions outside of clouds to evaluate the agreement between the two water measurements and (ii) we use the difference between H_2O_{enh} and H_2O_{gas} to determine whether a data point is inside or outside of a cirrus cloud.

2.1.1 H_2O data quality

Figure 1 shows examples of a comparison between the water instruments during some representative flights (a list of all flights is given in Table 3). The upper panel shows a flight with good agreement during mid-latitude CIRRUS 2006. The dark blue curve represents H_2O_{enh}, green is the original H_2O_{gas} measurement $H_2O_{gas,orig}$ and black $H_2O_{sat,ice}$. The cyan line is $H_2O_{gas,adj}$ that is determined by adjusting the $H_2O_{gas,orig}$

measurement to H_2O_{enh} in clear air. We choose as the reference the H_2O_{enh} observations because the FISH is the only instrument that was calibrated in the laboratory before and after each field campaign and in the field before every flight. For the flight shown here the cyan and green data points nearly match each other and this data set is classified as a "good flight". This good agreement is very often found in regions where the H_2O content is larger than about 10 ppmv. In such cases $H_2O_{gas,orig}$ is used as final H_2O_{gas}.

The middle panel shows data from a flight during SCOUT 2005 at water vapour values lower than about 5 ppmv. At these low values, larger differences between the instruments are observed more frequently. The adjusted data points (cyan) are somewhat higher than the measured (orange), but the differences are nearly constant and the course of the two measurements correspond to each other. Thus, this flight is classified as 'acceptable' and the $H_2O_{gas,adj}$ is used as H_2O_{gas} for further analysis.

The lowest panel shows a flight also at low water vapour, during TROCCINOX 2005. This is an example of a flight classified as 'bad' and rejected from the data base as a result of the large scatter between the adjusted and measured values. This means that the characteristics of the two instruments do not match which is a criterion to discard a flight.

This data quality check procedure was applied to 37 flights (listed in Table 3) where both H_2O_{enh} and $H_2O_{gas,orig}$ measurements are available. Nine flights were eliminated so that the data base for further analysis of RH_{ice} contains 28 flights (see Sect. 3.1).

2.1.2 Cloud detection

After the data quality check was applied, the water vapour measurements were evaluated to determine if the aircraft was in or out of a cloud. For this purpose, ice crystal measurements from the optical particle probes were often used; however, given that these instruments were not always available, a complementary technique was applied that incorporated only the measurements from the water vapour instruments. From the processed H_2O_{gas} we calculate RH_{ice} and from H_2O_{enh} we determine $RH_{ice,enh}$. The

latter represents gas phase water plus the over-sampled ice crystals expressed as relative humidity (see Table 2). The ratio $RH_{ice,enh}/RH_{ice}$ is used as "cirrus-parameter" from which two regimes of cirrus are defined:

Cirrus regime (a) where $RH_{ice,enh}/RH_{ice}>1$ and $RH_{ice,enh}>100\%$. This regime represents a supersaturated cirrus. In Fig. 2, a part of the "good flight" of Fig. 1 (Cirrus 2006, November 29) is shown. In Fig. 1 it is seen that both measurements, H_2O_{enh} and H_2O_{gas} show a scatter that makes it difficult to explicitly state if a data point is inside cirrus, especially when $RH_{ice,enh}/RH_{ice}$ only slightly exceeds 1. Therefore, we discriminate three cirrus classes, differing by the uncertainty of the data points inside the cirrus. In Fig. 2, RH_{ice} is colour coded for the three classes: 1) if $RH_{ice,enh}/RH_{ice}>1.3$ (cyan), a data point is confidently inside cirrus, 2) if $RH_{ice,enh}/RH_{ice}=1.07-1.3$ (yellow) it is less confident and 3) when $RH_{ice,enh}/RH_{ice}=1.0-1.07$ (red) it is uncertain whether those measurements were inside the cloud. $RH_{ice,enh}$ is plotted in blue and RH_{ice} outside of cirrus in green. As already discussed by Schiller et al. (2008) the data points of the third class ($RH_{ice,enh}/RH_{ice}=1.0-1.07$) are not inside of cirrus in most cases, whereas most of the measurements in the second class are inside of cirrus.

Cirrus regime (b) whereby $RH_{ice,enh}/RH_{ice}>1$ and $RH_{ice,enh}<100\%$. These situation maybe caused by a subsaturated cirrus, but might also be the result of the scatter of the water vapour. Here, we define this as cirrus only when $RH_{ice,enh}/RH_{ice}>1.3$.

All data points not matching the criterions (a) or (b) are defined as outside of cirrus. However, most of the observed data point are "confident" and, moreover, the "less confident" and "uncertain" data points do not influence the general picture of supersaturations.

2.1.3 Measurement uncertainties

The estimated uncertainties are estimated by Gaussian error propagation and are listed in Table 2.

The calculated uncertainty of RH_{ice} is in the range 12–17%. However, as discussed above, although state-of-the-art, high precision water instruments are used here, the

different H_2O measurements are not always in agreement, especially for aircraft observations, and we adjust $H_2O_{gas,orig}$ measurements to H_2O_{enh} from the FISH. The differences in RH_{ice} before the adjustment can be much higher than the estimated uncertainties, particularly at low temperatures.

We would like to emphasize here the need for further improvement of water vapour instrumentation, e.g. higher precision, sensitivity and time resolution, especially for aircraft measurements at low temperatures. A number of scientific questions related to water vapour in the atmosphere will remain unanswered without such.

2.2 Ice crystals

For our data analysis, we also use measurements of total ice crystals numbers concentration made from instruments mounted on the M55 Geophysika and the *envisCope*-Learjet using either a FSSP 100 or 300 (de Reus et al. (2008) and references herein). The flights are listed in Table 3. FSSP 100/300 sample particles in the size range 1.5–30/0.3–20 µm radius, so that ice crystals larger than this size range will not be detected. Given this limitation, the total number and mean size of ice crystals, N_{ice} and R_{ice}, are likely underestimated. The error in N_{ice} is small, because larger ice crystals are much less frequent than smaller ones, but the error in R_{ice} could be significant. Therefore, we here estimate R_{ice} from the IWC detected by the FISH (the FISH samples all ice crystals larger than 2 µm radius, Krämer and Afchine, 2004) together with N_{ice} from FSSP by assuming that all crystals are spheres of the same size (see Table 2).

Shattering of ice crystals on the inlet of the FSSP can lead to an overestimate of the ice crystal concentration and IWC (Gardiner and Hallett, 1985; Field et al., 2003; Field et al., 2006; McFarquhar et al., 2007). This is valid for clouds where the ice crystal population contains particles larger than approximately 50 µm (Baumgardner 2007, personal communication). Our measurements of R_{ice} in the temperature range 184–240 K lie mostly between 3–30 µm, while N_{ice} ranges from 0.005 to 60 cm^{-3} (see Sect. 3.4). Therefore we assume, in agreement with de Reus et al. (2008), that it is not

likely that shattering has significantly influenced the measurements presented in this study.

3 Results and discussion

3.1 Cirrus field observations

Altogether, 20.8 (about 14 150 km) and 15.4 h (about 10 470 km) of flight time was spent in clear sky and inside of cirrus, respectively. Inside of cirrus, a wide range of conditions at different latitudes (20° South to 75° North), altitudes (6–20 km) and temperatures (183–250 K) is spanned. The observations include frontal and lee wave cirrus in the Arctic and at mid-latitudes, while in the tropics ice crystals stemming from convection and convective outflow as well as subvisible cirrus layers are probed equally. Note here that we assume that the cirrus observations are not biased by the flight pattern. In most of the flights, the aircraft probed the cirrus clouds from top to bottom.

The original field measurements of RH_{ice} derived from $H_2O_{gas,orig}$ in- and outside of cirrus for all 37 flights with complete H_2O measurements (listed in Table 3) are plotted versus temperature in the top panels of Fig. 3. The data are sorted for in- and outside of cirrus and the H_2O quality check procedure is applied to all flights as described in Sect. 2.1. The processed data are presented in the bottom panels of Fig. 3. Comparison of the processed with the original RH_{ice} show that for temperatures above about 200 K all supersaturations above the homogeneous freezing threshold disappear for both in- and outside of cirrus observations. Below 200 K, a few supersaturations slightly above the homogeneous freezing threshold are found, which will be discussed in Sects. 3.2 and 3.3.

Comparison of our processed RH_{ice} data set with former field measurements during INCA 2000 (10 flights, Ovarlez et al. (2002)) and CRYSTAL FACE 2002 (10 flights, Gao et al., 2004) firstly shows that the temperature range of the cirrus observations during CRYSTAL FACE (~195–215 K) complements the range of INCA (~215–250).

In this temperature range the general picture from all measurements is that RH_{ice} is distributed between subsaturated and supersaturated values close to the homogeneous freezing threshold.

Closer comparison of our clear sky RH_{ice} field observations with those from the INCA campaign yields that the INCA RH_{ice} observations are slightly below our measurement range (Fig. 2 in Ovarlez et al. (2002)). We explain this feature with a higher time resolution of the in/outside of cloud criterion, which is 1 s here and 7 s for INCA. That means, the INCA data points are more distant from the cirrus and thus, assuming that the highest RH_{ice} are reached immediately before the point of cirrus formation, lower supersaturation seems to be consequent.

Gao et al. (2004) (their Fig. 1) averaged in-cloud supersaturations from CRYSTAL FACE and proposed an average of 110% for temperatures above around 205 K, rising to around 130% for lower temperatures. The enhanced supersaturation at low temperatures are explained by diminished H_2O uptake of the ice crystals which is caused by HNO_3 deposits on the ice surface. From our measurements, showing a higher data density and extending the temperature range of CRYSTAL FACE down to 182 K, we cannot confirm a constant supersaturation in the two temperature ranges.

Further discussion of the structure of the RH_{ice} clear sky and in-cloud observations is provided in Sects. 3.2 (Clear sky RH_{ice}), 3.3 (RH_{ice} inside of cirrus).

3.2 Clear sky RH_{ice}

Under clear sky conditions, supersaturations up to the freezing thresholds of the available aerosol particles may occur in the upper troposphere (see Introduction). From our clear sky observations in the vicinity of cirrus clouds (Fig. 3, bottom right panel and, as frequencies of occurrence, in Fig. 4), representing 15.9 h of aircraft flight time, it can be seen that for temperatures>200 K RH_{ice} randomly distributes between nearly zero up to the homogeneous freezing thresholds. This finding is in agreement with Ovarlez et al. (2002), deriving a frequency distribution for mid-latitude cirrus clouds covering the temperature range 215–235 K from the INCA field experiment.

For lower temperatures, the upper limit of RH_{ice} is in general also the homogeneous freezing line, but a few data points are found slightly above (see Sect. 3.2). The lower RH_{ice} limit is enveloped by the dashed line in Fig. 3 (bottom right panel), representing a constant H_2O value of 1.5 ppmv, the minimum water vapour mixing ratio observed in the upper tropical troposphere. The highest frequencies of occurrence of RH_{ice} are enclosed by the dashed lines in Fig. 4, representing constant values of 2 and 3 ppmv which correspond to the upper tropospheric range of water vapour mixing ratios.

No supersaturations close to or above water saturation are observed in our field measurements. Thus, from our data set we could not confirm the hypothesis of severe suppression of ice cloud formation as given by Jensen et al. (2005b), showing clear sky RH_{ice} up to 230% at 187 K. Nevertheless, below 200 K a few cases of supersaturations slightly above the homogeneous freezing threshold are observed, raising the question if at these low temperatures the freezing of liquid aerosol particles may occur at higher supersaturations as described by Koop's theory.

Murphy et al. (2007) reported that around 50% of the aerosol particles in the cold uppermost troposphere contain organic material. Ice nucleation experiments at the AIDA chamber with soot and mineral dust particles containing organic material show that the heterogeneous freezing process of these particles is hindered (Möhler et al., 2005b; Möhler et al., 2008). In a model study, Kärcher and Koop (2005) show that homogeneous freezing of solution droplets is hindered in the presence of organics. Laboratory experiments for homogeneous freezing (Beaver et al., 2006) of sulfuric acid aerosols containing differing organic substances show both, increasing and decreasing ice nucleation temperatures in dependence on the organic compound. Recent studies of Murray (2008) and Zobrist et al. (2008) investigate the suppression of homogeneous ice crystallisation at low temperatures in highly viscous aqueous organic acid droplets or glass forming aerosol particles. Considering these studies together with our clear sky field observations yield a consistent picture. A further discussion of the freezing suppression is given in Sect. 3.5.

3.3 In-cloud RH_{ice}

Immediately after ice formation, but already inside of an ice cloud, the supersaturation is close to the freezing threshold. In the further cirrus life time, RH_{ice} will, depending on the ice clouds microphysical and thermodynamical development, adjust to equilibrium in accordance with the water exchange with the ice crystals.

The RH_{ice} field data inside of cirrus are shown in Fig. 3 (bottom left panel). Values of RH_{ice} between around 50% and the homogeneous thresholds are found. The lower RH_{ice} limit seems to decrease with decreasing temperature, except two strokes at around 220 and 230 K dropping down to near zero. These observations stem from flights in tropical thick (SCOUT-O_3 2005, Darwin) cirrus at around 14/11 km. Both observations were at the very close edge of the cirrus, maybe in the transition zone between in/outside of cirrus. The decrease with temperature of the lowest RH_{ice} may be explained with longer evaporation times at lower temperatures, causing the ice crystals to survive longer during the evaporation stage of the cloud.

Below 200 K, no supersaturations close to or above water saturation are observed in our field measurements, but a few RH_{ice} data above the homogeneous freezing line are found as in the clear sky data set. They may either portrait the higher freezing thresholds discussed in Sect. 3.2, or represent the so called "peak RH_{ice}" in very young, thin cirrus. This peak RH_{ice} is described by Kärcher and Lohmann (2002) and is seen in heterogeneous ice nucleation experiments at the aerosol chamber AIDA for soot particles coated with sulfuric acid (Möhler et al., 2005a), soot containing organic carbon (Möhler et al., 2005b) and mineral dust particles (Möhler et al., 2006): after ice crystal formation and continuous cooling, RH_{ice} still rises up to the peak RH_{ice}. This further increase in RH_{ice} is because the ice crystals are so small or so few in the beginning, that the water depletion of the gas phase is not large enough to compensate the increase of RH_{ice} caused by the further cooling. The duration and the degree of the post-ice nucleating RH_{ice} increase inversely depend on the number of ice crystals, because fewer ice crystals consume the water vapour much slower and therefore RH_{ice} can

raise higher. In colder ice clouds, this behaviour becomes more pronounced.

3.4 Cirrus in dynamical equilibrium

To further explain the pattern of RH_{ice} inside of cirrus we elaborate simple, observation based theoretical considerations of supersaturations in dynamical equilibrium of cirrus.

Dynamical equilibrium ("quasi steady state") in ice clouds is described by Korolev and Mazin (2003) as the state where changes in the mean size of the ice particles ($\overline{R_i}$) can be neglected and the ice particle number (N_i) and vertical velocity (u_z) are nearly constant. Then, changes in supersaturation are zero $\frac{dRH_{ice}}{dt}=0$ because the gas phase depletion of water by transport to the ice crystals compensates the decrease of the saturation water vapour pressure caused by the cooling. Korolev and Mazin (2003) describe the dynamical equilibrium supersaturation RH_{qsi} as

$$RH_{qsi} = \frac{u_z}{N_i \overline{R_i}} \cdot \frac{a_0}{b_i} - \frac{b_i^*}{b_i} \tag{1}$$

a_0, b_i, b_i^* are parameters depending on temperature, pressure, etc., and $N_i\overline{R_i}$ is the integral ice particle radius.

The time the initial in-cloud supersaturation, which is close to the freezing threshold, needs to reach the dynamical equilibrium is the relaxation time τ:

$$\tau = \frac{1}{a_0 \cdot u_z + (b_i + b_i^*)(N_i \overline{R_i})} \tag{2}$$

The main parameters influencing RH_{qsi} and τ are $N_i\overline{R_i}$, u_z, T (and p, but in the upper tropospheric pressure range this influence is negligible).

From our data set of cirrus ice crystal number densities N_{ice} and sizes R_{ice} observed during 20 flights (Fig. 5; measurement techniques are described in Sect. 2.2), we can derive atmospheric values of $N_i\overline{R_i}$. Firstly, $N_i\overline{R_i}$ are identified by encompassing the

observed ranges by lines for the minimum (N_{ice}: yellow, R_{ice}: green), the middle (both red) and the maximum (N_{ice}: green, R_{ice}: yellow). Secondly, because the number of ice crystals is roughly inversely linked to their size, the N_{ice} and R_{ice} lines of the same colour are multiplied:

$$N_i R_i \text{min} = N_{ice,min} \cdot R_{ice,max}, \quad (3)$$

$$N_i R_i \text{middle} = N_{ice,middle} \cdot R_{ice,middle}, \quad (4)$$

$$N_i R_i \text{ max} = N_{ice,max} \cdot R_{ice,min}. \quad (5)$$

By knowing now the minimum, mean and maximum of $N_i R_i$ in dependence on temperature, we calculated the corresponding RH_{qsi} and τ for two vertical velocities u_z, respectively (Fig. 6). A higher and a low u_z are chosen for the different $N_i R_i$ (thick, medium and thin cirrus) to represent on the one hand a young cirrus directly after formation and on the other hand an older cirrus at the end of its lifetime. We used differing u_z for each of the three cloud types, because for the frequently occuring homogeneous ice formation process the ice crystal number increases with increasing updraft, i.e. thick clouds are formed at high u_z and thin cirrus at low u_z (see also Sect. 3.5). Hence, u_z of 300 and 3 cm/s (dashed and dashed-dotted green lines) are chosen for the maximum $N_i R_i$, 30/1 cm/s for middle $N_i R_i$ (red lines) and 3/0.1 cm/s for the minimum $N_i R_i$ (yellow lines).

In young cirrus with higher u_z, the dynamical equilibrium RH_{qsi} tends to supersaturations over the complete temperature range for thick, medium as well as thin cirrus (dashed green, red and yellow lines in Fig. 6, left; note that natural cirrus cannot reach dynamical equilibrium when the time scale of changes in u_z are shorter than τ, which is the case very often). But, the supersaturations strongly increases with decreasing temperatures. This increase is caused mainly by the decrease of $N_i R_i$ with decreasing temperature, combined with the effect that the water vapour transport slows down with decreasing temperature. Together, the gas phase depletion of water by transport to the ice crystals cannot completely compensate the fast decrease of the saturation water vapour pressure. Enhanced time is needed to transport the water vapour in case

ACPD
8, 21089–21128, 2008

of fewer ice crystals are present. Thus, the relaxation times to reach the dynamical equilibrium greatly differ with the ice crystal number: for thick ice clouds (green dashed line in Fig. 6, right), dynamical equilibrium is reached very quickly in the timescale of 0.3–2 s with decreasing temperature, for medium clouds the relaxation time raises to 4 s–20 min and thin ice clouds needs and 1–3 h to relax to equilibrium. That means, at low temperatures saturation inside of ice clouds can hardly be reached as long as the cloud is further cooled.

Intensifying the cooling rate would force RH_{qsi} towards higher RH_{qsi} (not shown here), while reducing of cooling forces RH_{qsi} towards saturation. However, a dynamical equilibrium RH_{qsi} of around 100% is only reached when u_z slows down to very low values in older thick, medium and thin ice clouds (Fig. 6, left, dashed-dotted lines). The timescales are nearly identical at higher temperatures and are a little longer at lower temperatures.

When comparing the calculated range of RH_{qsi} with the supersaturations observed inside of cirrus (Fig. 3, bottom left panel) it must be taken into account that before reaching dynamical equilibrium the supersaturations in cirrus are higher, because they start at the freezing threshold at the formation of the cloud. Then, the comparison shows that for the range of $N_i R_i$ considered here the observed supersaturations can be explained by conventional microphysics.

3.5 Frequencies of supersaturations and ice crystal numbers

As for the clear sky data set, frequencies of occurrence of in-cloud RH_{ice} binned in 1 K temperature intervals are derived from the field observations shown in Fig. 3 (bottom left panel) and plotted in Fig. 7. In Fig. 8, the frequency distributions of RH_{ice} are binned into two temperature ranges, namely larger and smaller than 205 K.

At temperatures larger than about 205 K, most of the RH_{ice} observations group around 100%. This finding is in agreement with the observations during the mid-latitude experiment INCA (Ovarlez et al. (2002), their Fig. 4 and Gayet et al. (2004), their Fig. 5). Higher supersaturations are less frequent and probably observed in young

cirrus directly after ice formation, while subsaturations are aged cirrus in the evaporation stage. The narrowness of the distribution is consistent with short water vapour relaxation times in this temperature range, causing these parts of the clouds life cycle to be short compared to the time the clouds live around saturation.

At temperatures lower than about 205 K, the grouping of the RH_{ice} frequencies of occurrence around saturation broadens, pointing to longer water vapour relaxation times than for the warmer cirrus. There is no clear supersaturation cycle during the cirrus lifetime in this temperature range.

To further investigate the RH_{ice} frequency distribution, frequencies of occurrence of N_{ice} (from Fig. 5) are derived similarly to the RH_{ice} frequencies and are shown in Fig. 9 (top panel). The minimum/middle/maximum N_{ice} from Fig. 5 are overlayed as thin solid lines.

The number of ice crystals that would form homogeneously for different constant vertical velocities u_z (1, 10, 100, 1000 cm/s) are shown as thick solid lines. They are calculated using a simple box model together with the ice microphysics as described in Spichtinger and Gierens (2008). Here, we assume only homogeneous nucleation with nucleation rates parameterised according to Koop et al. (2000) and a background concentration of sulphuric acid aerosol of N_a=300 cm^{-3}, which is typical for upper tropospheric conditions (see e.g. Minikin et al., 2003). The calculated ice crystal number concentrations can be interpreted as an upper limit for the amount of ice crystals formed in updrafts of this magnitude under atmospheric conditions.

The most obvious feature of Fig. 9 (top panel) is that the numbers of ice crystal formed by homogeneous freezing increase with decreasing temperature for each u_z, while the most frequent observed N_{ice} decreases, confirming and extending the observations of Gayet et al. (2006) in the temperature range 210–260 K during the INCA experiment.

In the following, we individually discuss the correlations between the numbers of ice crystals, supersaturations, vertical velocities u_z and relaxation times τ for the two supersaturation regimes separated at ~205 K. Each temperature regime represents

around 5 h of observations.

3.5.1 Warm cirrus (>205 K)

The observed grouping of RH_{ice} around 100% (Fig. 7) indicates short water vapour relaxation times, which occurs in case of high ice crystal numbers N_{ice} (Sect. 3.4).

Indeed, high N_{ice} observations (0.5–10 cm^{-3}) are most frequent at 225–240 K (Fig. 9, top panel). If homogeneous freezing is assumed to be the pathway of cloud formation, this corresponds to u_z between 10 and 100 cm/s or higher, as can be seen from the thick solid lines in Fig. 9 (top panel). This is in in good agreement with the studies of Gayet et al. (2006) as well as Kärcher and Ström (2003), the latter reporting 1–10 cm^{-3} ice crystals and an updraft speed of 10–100 cm/s in young cirrus observed in the temperature range 215–235 K during the INCA experiment. For such conditions, the relaxation times τ are in the range of minutes. The u_z and τ ranges are estimated from the data set of $N_{ice}\overline{R_{ice}}$ and RH_{ice} using Eqs. (1) and (2) (see also Fig. 6).

At about 205–225 K, middle N_{ice} (0.05–1 cm^{-3}) observations are most frequent, corresponding to u_z around 5–10 cm/s. Here, τ is a little longer and ranges up to several ten minutes, but still short enough to efficiently reduce the initial in-cloud supersaturations.

3.5.2 Cold cirrus (<205 K)

As mentioned above, in the cold temperature regime no clear supersaturation pattern can be seen in Fig. 7, implying that the water vapour relaxation times are longer here. Such long relaxation times can be caused by the slower water vapour diffusion in this temperature range, or, more important, low ice crystal numbers and/or high vertical velocities (see Sect. 3.4).

Very low N_{ice} observations (0.005–0.2 cm^{-3}) are most frequent at temperature below 205 K (Fig. 9, top panel). Higher ice crystal numbers are found only occasionally in the upper part of convective systems (note here that the time of observation in subvisible

and convective cirrus is equal, i.e. the N_{ice} pattern is not biased by differing sampling time).

The very low N_{ice} would correspond to u_z around or lower than 1 cm/s – in case they are formed by homogeneous freezing – and relaxation times τ from hours to a day. The u_z range is visible in Fig. 9, top panel: the most frequent ice crystal numbers group around and below the N_{ice}-line for u_z=1 cm/s. As a consequence, the time the water vapour needs to migrate to the few ice crystals after ice formation is so long that the high initial supersaturations, which correspond to the freezing thresholds, can be maintained over a longer period. Likewise, evaporation of ice crystals in a subsaturated environment occurs on a longer timescale. These considerations corroborate that the observations of persistent high in-cloud supersaturations in cold cirrus can be explained by conventional ice microphysics, with unexpectedly low ice crystal numbers.

Our observations are consistent with others, for example Lawson et al. (2008) report an N_{ice} range of 0.002–0.19 cm^{-3} at 188 to 198 K from 2.4 h of observation time in subvisible cirrus during the CR-AVE field campaign. Lawson et al. (2008) attributed the simoultaneous observations of high RH_{ice} to the colder temperatures and aerosol chemistry in the upper TTL compared to mid-latitude cirrus.

Two model case studies simulating cirrus observations during CRYSTAL-FACE (Khvorostyanov et al., 2006), and CR-AVE (Gensch et al., 2008) also show few ice crystals and state that high supersaturations at low temperature maybe explained under the assumption of heterogeneous freezing. In addition, Jensen et al. (2008) report in another CR-AVE model case study that the observation of few large crystals would not have been possible in the presence of homogeneous freezing.

Several scenarios are possible to explain the low ice crystal numbers: (i) the ice clouds have formed homogeneously at very low u_z (around or lower 1 cm/s), (ii) they formed via heterogeneous ice nucleation, (iii) ice nucleation is suppressed at low temperatures (see Sect. 3.2).

Scenario (i), homogeneous freezing at very low u_z, seems unlikely, because higher u_z do occur in the uppermost troposphere (Lawson et al., 2008; Jensen et al.; 2008).

Approach (ii), heterogeneous freezing as sole ice nucleating mechanism, is possible (see Khvorostyanov et al., 2006 and Gensch et al., 2008), but the question arises if this mechanism is the most frequent in the UT. In this case the homogeneous freezing threshold would rarely been reached after heterogeneous freezing once has occured. Another possible candidate is (iii), the supression of ice nucleation as discussed above. In case half of the particles contain organic material (Murphy et al., 2007), this could be a general mechanism. Perhaps all three ice forming processes occur in the uppermost troposphere with probabilities increasing from (i) to (iii).

4 Conclusions

We studied the upper tropospheric humidity in- and outside of cirrus clouds, motivated by the current discussion of persistent supersaturations up to or even above water saturation reported in recent years especially at low temperatures (Peter et al., 2006; 2008). A variety of hypotheses are discussed to understand the observations, but a key question raised in these studies is the quality of the water measurements. We here presented an extensive in-situ data set of strongly quality checked clear sky and in-cloud aircraft observations of relative humidity as well as ice crystal numbers in the temperature range 183–250 K (see Sect. 2).

In clear sky and inside of cirrus clouds we observed explicable supersaturations up to the homogeneous freezing threshold over the complete temperature range. At T<200 K, a small fraction of supersaturations slightly above the homogeneous freezing threshold but well below water saturation are found. The observations allow the following conclusions:

Clear sky supersaturations: From our robust data set cases of slight freezing suppression in cold ice clouds could be derived (see Sect. 3.2), but a severe suppression of ice formation that rises the clear sky supersaturation to values above water saturation is not seen. We support the idea that this freezing suppression is caused by the composition of the aerosol particles. We do not rule out here an impact of other hy-

pothesis to explain high supersaturations (see Peter et al., 2006 and Peter et al., 2008), such as a low mass accommodation of H_2O on aerosol particles or an underestimation of the vapour pressure of supercooled water, but altogether we do not observe a large effect on the ice formation in the upper troposphere.

In-cloud supersaturations: Likewise, no processes severely hindering the growth of ice crystals while holding up the supersaturation are necessary to explain our observations inside of clouds (see Sects. 3.3 and 3.4). But, as for clear sky, we do not rule out the possibility that several mechanisms discussed by Peter et al. (2006) and Peter et al. (2008) might influence the depletion of water vapour by growing ice crystals: a low mass accommodation of H_2O on ice, nitric acid deposition on ice forming NAT or cubic ice formation. However, from our data set we can not deduce a large effect on ice growth.

Supersaturations and ice crystal numbers: Persistent high – but below the homogeneous freezing threshold – supersaturations at low temperatures are found in our measurements. The key parameter explaining these observations is the number of ice crystals, which is unexpectedly low in most cases (see Sect. 3.5). Several scenarios are proposed to explain these low ice crystal numbers: (i) the ice clouds have formed homogeneously at very low u_z (around or lower 1 cm/s), (ii) they formed via heterogeneous ice nucleation, (iii) ice nucleation is suppressed at low temperatures. We speculate that all three ice forming processes occur in the uppermost troposphere with differing probabilities.

Considering this hypothesis together with our clear sky and in-cloud supersaturation as well as ice crystal number field observations yield a consistent picture for low temperatures: a combination of the different ice forming processes would produce clear sky and in-cloud supersaturations up to values above the homogeneous freezing threshold as well as low ice crystal numbers, which in turn causes persistent super- and subsaturations.

In summary, we confirm the existence of supersaturations up to the homogeneous freezing threshold and sometimes slightly above in- and outside of cirrus clouds. We

explain the observations with conventional knowledge of cloud microphysics. Especially, high persisent supersaturations at low temperatures are traced back to low ice crystal numbers which however are not yet fully understood.

Acknowledgements. We would like to thank Alexei Korolev for fruitful discussions and for leaving us the code for the dynamical equilibrium calculations. Thomas Peter is kindly acknowledged for stimulating continuous debates. We also greatfully acknowledge J. Beuermann, M. Bläsner, O. Bujok, N. Eicke, S. Rohs, F. H. Silva dos Santos, A. Schönfeld, V. Tan and M. Zöger who were involved in the experimental work during the different campaigns, as well as the aircraft teams of DLR Oberpfaffenhofen, GfD Hohn, *enviscope* Frankfurt and MDB Moscow and the coordinators of the different field experiments. Funding for the campaigns was granted by the BMBF within the Ozonforschungsprogramm and the programme "Angewandte Klima- und Atmosphärenforschung", by the EU DG XII within Framework Programmes 5 and 6, and by ESA within the ENVISAT validation programme. Water vapor measurements by FLASH and data preparation was supported by the Russian foundation for basic research grants No. 06-05-64165-a and 07-05-00486-a.

References

Beaver, M. R., Elrod, M. J., Garland, R. M., and Tolbert, M. A.: Ice nucleation in sulfuric acid/organic aerosols: implications for cirrus cloud formation, Atmos. Chem. Phys., 6, 3231–3242, 2006, http://www.atmos-chem-phys.net/6/3231/2006/. 21100

Comstock, J., Ackerman, T. P., and Turner, D.: Evidence of high ice supersaturation in cirrus clouds using ARM Raman lidar measurements, Geophys. Res. Lett., 31, L11106, doi:10.1029/2004GL019705, 2004. 21092

de Reus, M., Borrmann, S., Heymsfield, A. J., Weigel, R., Schiller, C., Mitev, V., Frey, W., Kunkel, D., Krten, A., Curtius, J., Sitnikov, N. M., Ulanovsky, A., and Ravegnani, F.: Evidence for ice particles in the tropical stratosphere from in-situ measurements, Atmos. Chem. Phys. Discuss., 8, 19313–19355, 2008, http://www.atmos-chem-phys-discuss.net/8/19313/2008/. 21097

Field, P., Heymsfield, A., and Bansemer, A.: Shattering and particle interarrival times measured by optical array probes in ice clouds, J. Atmos. Ocean. Tech., 23, 1357–1371, 2006a. 21097

Field, P., Wood, R., Brown, P., Kaye, P. H., Hirst, E., Greenaway, R., and Smith, J.: Ice particle interarrival times measured with a fast FSSP, J. Atmos. Ocean. Tech., 20, 249–261, 2006b. 21097

Gao, R., Popp, P., Fahey, D., Marcy, T., Herman, R., Weinstock, E., Baumgardener, D., Garrett, T., Rosenlof, K., Thompson, T., Bui, P., Ridley, B., Wofsy, S., Toon, B., Tolbert, M., Kärcher, B., Peter, T., Hudson, P., Weinheimer, A., and Heymsfield, A.: Evidence that nitric acid increases relative humidity in low-temperature cirrus clouds, Science, 303, 516–520, 2004. 21092, 21098, 21099, 21117

Gardiner, B. and Hallett, J.: Degradation of in-cloud forward scattering spectrometer probe measurements in the presence of ice particles, J. Atmos. Ocean. Tech., 2, 171–180, 1985. 21097

Gayet, J.-F., Ovarlez, J., Shcherbakov, V., Ström, M., Schumann, U., Minikin, A., Auriol, F., Petzold, A., and Monier, M.: Cirrus cloud microphysical and optical properties at southern and northern midlatitudes during the INCA experiment, J. Geophys. Res., 109, D20206, doi:10.1029/2004JD004803, 2004. 21092, 21104, 21117

Gayet, J.-F., Shcherbakov, V., Mannstein, H., Minikin, A., Schumann, U., Ström, J., Petzold, A., Ovarlez, J., and F., I.: Microphysical and optical properties of midlatitude cirrus clouds observed in the southern hemisphere during INCA experiment, Q. J. Roy. Meteor. Soc., 132, 2719-2748, doi:10.1256/qj.05.162, 2006. 21092, 21105, 21106

Gensch, I., Bunz, H., Baumgardner, D., Christensen, L., Fahey, D., Hermann, R., Lawson, P., Popp, P., Smith, J., Webster, C., Weinstock, E., Wilson, J., Peter, T., and Krämer, M.: Supersaturations, microphysics and nitric acid partitioning in a cold cirrus observed during CR-AVE 2006: An observation-modeling intercomparison study, Envir. Res. Lett., 3, doi:10.1088/1748-9326/3/3/035003, 2008. 21091, 21107, 21108

Gettelman, A. and Kinnison, D. E.: The global impact of supersaturation in a coupled chemistry-climate model, Atmos. Chem. Phys., 7, 1629–1643, 2007, http://www.atmos-chem-phys.net/7/1629/2007/. 21091

Gettelman, A., Fetzer, E., Eldering, A., and Irion, F.: The global distribution of supersaturation in the upper troposphere from the atmospheric infrared sounder, J. Climate, 19, 6089-6103, 2006. 21092, 21117

Gierens, K., Schumann, U., Helten, M., Smit, H., and Marenco, A.: A distribution law for relative humidity in the upper troposphere and lower stratosphere derived from three years of MOZAIC measurements, Ann. Geophys., 17, 1218–1226, 1999,

http://www.ann-geophys.net/17/1218/1999/. 21092, 21117
Gierens, K., Schumann, U., Helten, M., Smit, H., and Wang, P.: Ice-supersaturated regions and subvisible cirrus in the northern midlatitude upper troposphere, J. Geophys. Res., 105, 22 743–22 753, 2000. 21091, 21092, 21117
Glückauf, E.: Notes on upper air hygrometry – II: On the humidity in the stratosphere, Q. J. Roy. Meteor. Soc., 71, 110–112, 1945. 21091
Haag, W., Kärcher, B., Ström, J., Minikin, A., Lohmann, U., Ovarlez, J., and Stohl, A.: Freezing thresholds and cirrus cloud formation mechanisms inferred from in situ measurements of relative humidity, Atmos. Chem. Phys., 3, 1791–1806, 2003, http://www.atmos-chem-phys.net/3/1791/2003/. 21092, 21117
Heymsfield, A. and Milosevitch, L.: Relative humidity and temperature influences on cirrus formation and evolution: obeservations from wave clouds and FIRE II, J. Atmos. Sci., 52, 4302–4326, 1995. 21092
Heymsfield, A., Miloshevich, L., and Twohy, C.: Upper-tropospheric relative humidity observations and implications for cirrus ice nucleation, Geophys. Res. Lett., 25, 1343–1346, 1998. 21092, 21117
Hoyle, C., Luo, B., and Peter, T.: The origin of high ice crystal number densities in cirrus clouds, J. Atmos. Sci., 62, 2568–2579, 2005. 21093
Immler, F., Treffeisen, R., Engelbart, D., Kruger, K., and Schrems, O.: Cirrus, contrails, and ice supersaturated regions in high pressure systems at northern mid latitudes, Atmos. Chem. Phys., 8, 1689–1699, 2008, http://www.atmos-chem-phys.net/8/1689/2008/. 21092, 21117
Jensen, E. et al.: Prevalence of ice-supersaturated regions in the upper troposphere: Implications for optically thin ice cloud formation, J. Geophys. Res., 106, 17 253–17 266, 2001. 21092, 21117
Jensen, E., Pfister, L., Bui, T., Weinheimer, A., Weinstock, E., Smith, J., Pittman, J., Baumgardner, D., and Lawson, P.: Formation of a tropopause cirrus layer observed over Florida during CRYSTAL-FACE, J. Geophys. Res., 110, doi:10.1029/2004JD004671, 2005a. 21092, 21117
Jensen, E., Smith, J., Pfister, L., Pittman, J., Weinstock, E., Sayres, D., Herman, R., Troy, R., Rosenlof, K., Thompson, T., Fridlind, A., Hudson, P., Cziczo, D., Heymsfield, A., Schmitt, C., and Wilson, J.: Ice supersaturations exceeding 100% at the cold tropical tropopause: implications for cirrus formation and dehydration, Atmos. Chem. Phys., 5, 851–862, 2005b, http://www.atmos-chem-phys.net/5/851/2005/. 21092, 21100, 21117

Jensen, E., Pfister, L., Bui, T., Lawson, P., Baker, B., Mo, Q., Baumgardner, D., Weinstock, E., Smith, J., Moyer, E., Hanisco, T., Sayres, D., St. Clair, J., Alexander, M., Toon, O., and Smith, J.: Formation of large (≃100 µm) ice crystals near the tropical tropopause, Atmos. Chem. Phys., 8, 1621–1633, 2008, http://www.atmos-chem-phys.net/8/1621/2008/. 21107

Kelly, K., Proffitt, M., Chan, R., Loewenstein, M., Podolske, J., Strahan, E., Wilson, J., and Kley, D.: Water vapor and cloud water measurements over Darwin during the STEP 1987 tropical mission , J. Geophys. Res., 98, 8713–8723, 1993. 21092, 21117

Khvorostyanov, V., Morrison, H., Curry, J., Baumgardner, D., and Lawson, P.: High supersaturation and modes of ice nucleation in thin tropopause cirrus: Simulation of the 13 July 2002 cirrus regional study of tropical anvils and cirrus layers case, J. Geophys. Res., 111, doi:10.1029/2004JD005235, 2006. 21091, 21107, 21108

Koop, T., Luo, B., Tsias, A., and Peter, T.: Water activity as the determinant for homogeneous ice nucleation in aqueous solutions, Nature, 406, 611–614, 2000. 21091, 21105, 21122, 21125, 21128

Korolev, A. and Mazin, I.: Supersaturation of water vapor in clouds, Am. Meteorol. Soc., 60, 2957–2976, 2003. 21093, 21102

Krämer, M. and Afchine, A.: Sampling characteristics of inlets operated at low U/U0 ratios: new insights from computational fluid dynamics (CFX) modeling, J. Aerosol Sci., 35, 683–694, 2004. 21097

Kärcher, B. and Koop, T.: The role of organic aerosols in homogeneous ice formation, Atmos. Chem. Phys., 5, 703–714, 2005, http://www.atmos-chem-phys.net/5/703/2005/. 21100

Kärcher, B. and Lohmann, U.: A parameterization of cirrus cloud formation: Homogeneous freezing of supercooled aerosols, J. Geophys. Res., 107(D2), 4010, doi:10.1029/2001JD000470 21101

Kärcher, B. and Ström, J.: The roles of dynamical variability and aerosols in cirrus cloud formation, Atmos. Chem. Phys., 3, 823–838, 2003, http://www.atmos-chem-phys.net/3/823/2003/. 21106

Lawson, R., Pilson, B., Baker, B., Mo, Q., Jensen, E., Pfister, L., and Bui, P.: Aircraft measurements of microphysical properties of subvisible cirrus in the tropical tropopause layer, Atmos. Chem. Phys., 8, 1609–1620, 2008, http://www.atmos-chem-phys.net/8/1609/2008/. 21107

Lee, S.-H., Wilson, J., Baumgardner, D., Herman, R., Weinstock, E., LaFleur, B., Kok, G., Anderson, B., Lawson, P., Baker, B., Strawa, A., Pittman, J., Reeves, J., and Bui, T.: New particle formation observed in the tropical/subtropical cirrus clouds, J. Geophys. Res., 109, 2004. 21092, 21117

MacKenzie, A., Schiller, C., Peter, T., Adriani, A., Beuermann, J., Bujok, O., Cairo, F., Corti, T., DiDonfrancesco, G., Gensch, I., Kiemle, C., Krämer, M., Rohs, S., Rudakov, V., Kroger, C., Merkulov, S., Oulanovsky, A., Ravegnani, F., Salter, P., Santacesaria, V., Stefanutti, L., and Yushkov, V.: Tropopause and hygropause variability over the equatorial Indian Ocean during February and March 1999, J. Geophys. Res., 111, D18112, doi:10.1029/2005JD006639, 2006. 21092, 21117

May, R. and Webster, C.: Data processing and calibration for tunable diode laser harmonic absorption spectrometers, J. Quant. Spectrosc. Ra., 49, 335-347, 1993. 21094

McFarquhar, G., Junshik, U., Freer, M., Baumgardner, D., Kok, G., and Mace, G.: The importance of small ice crystals to cirrus properties: Observations from the tropical warm pool international cloud experiment (TWP-ICE), Geophys. Res. Lett., 34, L13803, doi:10.1029/2007GL029865, 2007. 21097

Minikin, A., Petzold, A., Ström, J., Krejci, R., Seifert, M., van Velthoven, P., Schlager, H., and Schumann, U.: Aircraft observations of the upper tropospheric fine particle aerosol in the Northern and Southern Hemispheres at midlatitudes, Geophys. Res. Lett., 30(10), 1503, doi:10.1029/2002GL016458, 2003. 21105

Möhler, O., Büttner, S., Linke, C., Schnaiter, M., Saathoff, H., Stetzer, O., Wagner, R., Krämer, M., Mangold, A., Ebert, V., and Schurath, U.: Effect of sulfuric acid coating on heterogeneous ice nucleation by soot aerosol particles, J. Geophys. Res., 110, D11210, doi:10.1029/2004JD005169, 2005a. 21101

Möhler, O., Linke, C., Saathoff, H., Schnaiter, M., Wagner, R., Mangold, A., Krämer, M., and Schurath, U.: Ice nucleation on flame soot aerosol of different organic carbon content, Meteorol. Z., 14, 477–484, 2005b. 21100, 21101

Möhler, O., Field, P. R., Connolly, P., Benz, S., Saathoff, H., Schnaiter, M., Wagner, R., Cotton, R., Krämer, M., Mangold, A., and Heymsfield, A. J.: Efficiency of the deposition mode ice nucleation on mineral dust particles, Atmos. Chem. Phys., 6, 3007–3021, 2006, http://www.atmos-chem-phys.net/6/3007/2006/. 21101

Möhler, O., Benz, S., Saathoff, H., Schnaiter, M., Wagner, R., Schneider, J., Walter, S., Ebert, V., and Wagner, S.: The effect of organic coating on the heterogeneous ice nucleation effi-

ciency of mineral dust aerosols, Environ. Res. Lett., 3, doi:10.1088/1748-9326/3/2/025007, 2008. 21100
Murphy, D., Cziczo, D., Hudson, P., and Thomson, D.: Carbonaceous material in aerosol particles in the lower stratosphere and tropopause region, J. Geophys. Res., 112, D04203, doi:10.1029/2006JD007297, 2007. 21100, 21108
Murray, B. J.: Inhibition of ice crystallisation in highly viscous aqueous organic acid droplets, Atmos. Chem. Phys., 8, 5423–5433, 2008, http://www.atmos-chem-phys.net/8/5423/2008/. 21100
Ovarlez, J., Gayet, J.-F., Gierens, K., Ström, J., Ovarlez, H., Auriol, F., Busen, R., and Schumann, U.: Water vapour measurements inside cirrus clouds in Northern and Southern hemispheres during INCA, Geophys. Res. Lett., 29(16), 1813, doi:10.1029/2001GL014440, 2002. 21092, 21098, 21099, 21104, 21117
Peter, T., Marcolli, C., Spichtinger, P., Corti, T., Baker, M., and Koop, T.: When dry air is too humid, Science, 314, 1399–1401, 2006. 21092, 21108, 21109
Peter, T., Krämer, M., and Möhler, O.: Upper Tropospheric Humidity: A Report on an International Workshop, SPARC Newsletter, 9–15, 2008. 21109
Popp, P., Marcy, T., Watts, L., Gao, R., Fahey, D., Weinstock, E., Smith, J., Herman, R., Troy, R., Webster, C., Christensen, L., Baumgardner, D., Voigt, C. Kärcher, B., Wilson, J., Mahoney, M., Jensen, E., and Bui, T.: Condensed-phase nitric acid in a tropical subvisible cirrus cloud, Geophys. Res. Lett., 34, L24812, doi:10.1029/2007GL031832, 2007. 21092, 21117
Schiller, C., Krämer, M., Afchine, A., Spelten, N., and Sitnikov, N.: The ice water content in Arctic, midlatitude and tropical cirrus, J. Geophys. Res., in press, 2008. 21094, 21096, 21125
Sitnikov, N., Yushkov, V., Afchine, A., Korshunov, L., Astakhov, V. I., Ulanovskii, A., Krämer, M., Mangold, A., Schiller, C., and Ravegnani, F.: The FLASH instrument for water vapor measurements on board the high-altitude airplane, Instrum. Exp. Tech., 50, 113–121, 2007. 21094
Spichtinger, P. and Gierens, K. M.: Modelling of cirrus clouds Part 1: Model description and validation, Atmos. Chem. Phys. Discuss., 8, 601–686, 2008, http://www.atmos-chem-phys-discuss.net/8/601/2008/. 21105
Spichtinger, P., Gierens, K., and Read, W.: The global distribution of ice supersaturated regions as seen by the microwave limb sounder., Q. J. Roy. Meteor. Soc., 129, 3391–3410, 2003. 21091, 21092, 21117

Spichtinger, P., Gierens, K., Smit, H. G. J., Ovarlez, J., and Gayet, J.-F.: On the distribution of relative humidity in cirrus clouds, Atmos. Chem. Phys., 4, 639–647, 2004, http://www.atmos-chem-phys.net/4/639/2004/. 21092, 21117

Vömel, H. and David, D. E., and Smith, K.: Accuracy of tropospheric and stratospheric water vapor measurements by the cryogenic frost point hygrometer: Instrumental details and observations, J. Geophys. Res., 112, D08305, doi:10.1029/2006JD007224, 2007. 21092, 21117

Wall, E.: Material zur Frage der Eiskeimbildung in der Atmosphäre, Meteorol. Z., 59, 109–120, 1942. 21091

Weickmann, H.: Formen und Bildung atmosphärischer Eiskristalle, Beitr. Phys. Atmos., 28, 12–52, 1945. 21091

Zobrist, B., Marcolli, C., Pedernera, D. A., and Koop, T.: Do atmospheric aerosols form glasses?, Atmos. Chem. Phys., 8, 5221–5244, 2008, http://www.atmos-chem-phys.net/8/5221/2008/. 21100

Zöger, M., Afchine, A., Eicke, N., Gerhards, M.-T., Klein, E., McKenna, D., Mörschel, U., Schmidt, U., Tan, V., Tuitjer, F., Woyke, T., and Schiller, C.: Fast in situ stratospheric hygrometers: A new family of balloon-borne and airborne Lyman-photofragment fluorescence hygrometers., J. Geophys. Res., 104, 1807–1816, 1999. 21094

Table 1. Observations of supersaturations in clear air and inside of cirrus clouds.

	Temperature (K)	Study	High ice-supersaturation in clear air	in-cloud
	$T > 200$			
Heymsfield and Milosevitch (1995)	220–240	aircraft in-situ: Wave90	frequent, up to hom. freezing threshold	frequent and substantial
Heymsfield et al. (1998)	205–240	aircraft and balloon in-situ: FIRE-II, SUCCESS	frequent occurrence, up to hom. freezing threshold occasionally above	
Jensen et al. (2001)	205–235	aircraft in-situ: SUCCESS, SONEX, POLINAT-2,CAMEX	frequent occurrence, up to hom. freezing threshold occasionally water saturation	
Gierens et al. (1999), Gierens et al. (2000)	>200	aircraft in-situ: MOZAIC and satellite: SAGE II	frequent occurrence, up to ~ 140%	
Ovarlez et al. (2002), Haag et al. (2003) Gayet et al. (2004), (2006)	210–240	aircraft in-situ: INCA	up to near hom. freezing threshold max. ~ 140%	up to hom. freezing threshold, max. ~ 150% occasionally above
Spichtinger et al. (2003)	>200	satellite: UARS MLS	globally frequent occurrence, up to ~ 140%	
Spichtinger et al. (2004)	219–239	aircraft in-situ: MOZAIC		up to ~ 140%, mean increases with decreasing T
Lee et al. (2004)	205-210	in-situ aircraft: CRYSTAL-FACE		in-cloud persistent 160%
Comstock and Ackerman (2004)	>200	groundbased: Raman lidar	occurrence, up to ~ 160%,	frequent occurrence, up to hom. freezing thresh., max. ~ 160%, increases with decreasing T
Gettelman et al. (2006)	>210	satellite: AIRS	globally frequent occurrence, max. ~ 250%,	
Immler et al. (2008)	200–240	groundbased: Raman lidar	frequent occurrence similar Ovarlez et al. (2002)	
	$T < 200$			
Kelly et al. (1993)	<195	in-situ aircraft: STEP	up to hom. freezing threshold, occasionally above	
Gao et al. (2004)	<205	in-situ aircraft: CRYSTAL-FACE		up to 160%
Jensen et al. (2005a)	198–204	in-situ aircraft: CRYSTAL-FACE		up to 180%
Jensen et al. (2005b)	187	in-situ aircraft: Pre-AVE	up to 230%	
MacKenzie et al. (2006)	185–195	in-situ aircraft: APE-THESEO	up to 140%	up to 170%
Popp et al. (2007)	185–190	in-situ aircraft: CR-AVE		persistent 230-250%
Vömel and David (2007)	185–235	in-situ balloon	frequent occurrence, up to hom. freezing threshold occasionally water saturation	

Table 2. Instruments and parameters used during aircraft experiments (FISH: Fast In-situ Stratospheric Hygrometer; OJSTER: Open path Jülich Stratospheric Tdl ExpeRiment, FLASH: Fluorescent Airborne Stratospheric Hygrometer, FSSP: Forward Scattering Spectrometer Probe; TDC: Thermo Dynamic Complex; all instruments except FSSP are operated at 1 Hz, FSSP at 2 Hz).

Quantity		Description	Instrument	Remarks	Uncertainty
H_2O_enh	(ppmv)	gas phase H_2O + enhanced ice	FISH*	*Lyman-a-hygrometer	6%±0.2 ppmv
$H_2O_{gas,orig}$	(ppmv)	original gas phase H_2O	FLASH*/OJSTER†	†Open path TDL	8%
$H_2O_{gas,adj}$	(ppmv)	adjusted gas phase H_2O	FISH,FLASH/OJSTER	see text	10–15%
H_2O_{gas}	(ppmv)	processed gas phase H_2O	FISH,FLASH/OJSTER	see text	10–15%
IWC	(ppmv)	Ice Water Content	FISH, FLASH/OJSTER	$\frac{H_2O_{enh}-H_2O_{gas}}{Enhancement}$	10–15%
RH_{ice}	(%)	Relative Humidity wrt ice	FISH,FLASH/OJSTER	$H_2O_{gas}/H_2O_{sat,ice}$	12–17%
$RH_{ice,enh}$	(%)	enhanced RH_{ice}	FISH	$H_2O_{enh}/H_2O_{sat,ice}$	9–14%
$H_2O_{sat,ice}$	(Pa)	H_2O vapour saturation wrt ice	Marti+Mauersberger (1993)	$10^{(.2663.5/T+12.537)}$	7%
T	(K)	Temperature	Avionik, TDC		0.5 K
p	(hPa)	Pressure	Avionik		1 hPa
N_{ice}	(cm^{-3})	Number of ice crystals	FSSP	Optical particle spectrometer	10–100%
R_{ice}	(μm)	Size of ice crystals	FSSP, FISH	$[IWC/N_{ice}\cdot 3/(4\pi\cdot\rho_{rice})]^{1/3}$	10–100%
			on board of DLR Falcon (12 km)	FISH, OJSTER, Avionik	
			enviscope-Learjet (14 km)	FISH, OJSTER, FSSP, Avionik	
			M55 Geophysica (20 km)	FISH, FLASH, FSSP, Avionik or TDC	

Table 3. List of 43 flights from 10 field campaigns using three aircraft (M55 Geophysika, *enviscope*-Learjet; DLR Falcon). For 37 flights both H_2O_{enh} (FISH) and H_2O_{gas} (FLASH or OJSTER) are available; 1/0 denotes the agreement of the H_2O measurements as described in Sect. 2 (1: agreed or adjusted, 0: no agreement, data are sorted out from the data base), and 20 flights with ice crystal measurements (FSSP) are performed. POLSTAR: Polar Stratospheric Aerosol Experiment, EUPLEX: European Polar Stratospheric Cloud and Lee Wave Experiment, ENVISAT: Envisat validation experiment , CIRRUS: Cirrus characterisation experiment, APE-THESEO: Third European Stratospheric Experiment on Ozone, TROCCINOX: Tropical Convection, Cirrus and Nitrogen Oxides Experiment, SCOUT-O_3: StratosphericClimate Links with Emphasis on the Upper Troposphere and Lower Stratosphere.

Campaign	Aircraft	Date	FISH + FLASH/OJSTER	FSSP	Location
			ARCTIC		
POLSTAR 1998	Learjet	0126-1		1	Kiruna, Sweden (68° N)
EUPLEX 2003	Geophysika	0115-1	1		Kiruna, Sweden (68° N)
	Geophysika	0126-1		1	
	Geophysika	0208-1	0		
	Geophysika	0209-1	1		
	Geophysika	0211-1		1	
ENVISAT 2003	Geophysika	0302-1	1	1	Kiruna, Sweden (68° N)
	Geophysika	0316-1	1	1	
			Mid-Latitude		
CIRRUS 2003	Learjet	1212-1	1		Hohn, Germany (54° N)
	Learjet	1213-1	1		
CIRRUS 2004	Learjet	1124-1	1	1	Hohn, Germany (54° N)
	Learjet	1127-1	1	1	
CIRRUS 2006	Learjet	1124-1	0	1	Hohn, Germany (54° N)
	Learjet	1127-1	0		
	Learjet	1128-1	1		
	Learjet	1128-2	1		
	Learjet	1129-1	1	1	
ENVISAT 2002	Geophysika	1008-1	1		Forli, Italy (44° N)
	Geophysika	1014-1	0		
	Geophysika	1017-1	0		
			Tropics		
APE-THESEO 1999	Geophysika	0219-1	1		Indian Ocean (5° S)
	Geophysika	0309-1	0		
SCOUT-O_3 2005	Geophysika	1107-1	1		Darwin, Australia (12° S)
	Geophysika	1109-1	1		
	Geophysika	1111-1	1		
	Geophysika	1112-1	1		
	Geophysika	1119-1	1	1	
	Geophysika	1123-1	1		
	Geophysika	1125-1		1	
	Geophysika	1129-1	0	1	
	Geophysika	1130-1	1	1	
	Geophysika	1130-2	1	1	
	Falcon	1128-1	1		
	Falcon	1129-1	1		
	Falcon	1130-2	1		
TROCCINOX 2005	Geophysika	0127-1	1		Araatuba, Brazil (21° S)
	Geophysika	0201-1	1		
	Geophysika	0204-1	0	1	
	Geophysika	0205-1		1	
	Geophysika	0208-1	0	1	
	Geophysika	0217-1		1	
	Geophysika	0218-1	1	1	
	Geophysika	0224-1	1	1	

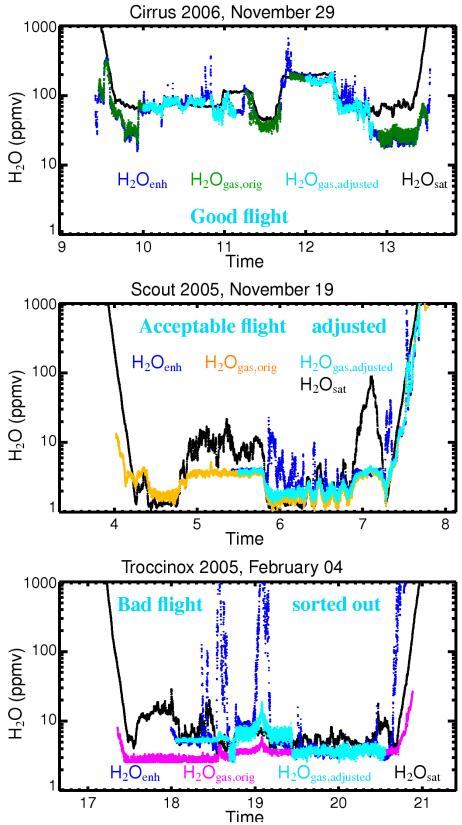

Fig. 1. H_2O data quality (upper panel: good flight; middle panel: acceptable flight; bottom panel: bad flight).

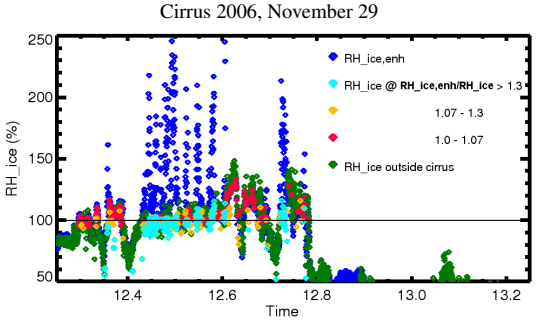

Fig. 2. RH_{ice} and $RH_{ice,enh}$ in the course of the flight Cirrus 2006, November 29, colour coded for "cirrus-parameter" $RH_{ice,enh}/RH_{ice}$ to define in/out cirrus (inside cirrus: confident, less confident, uncertain; outside cirrus).

ACPD
8, 21089–21128, 2008

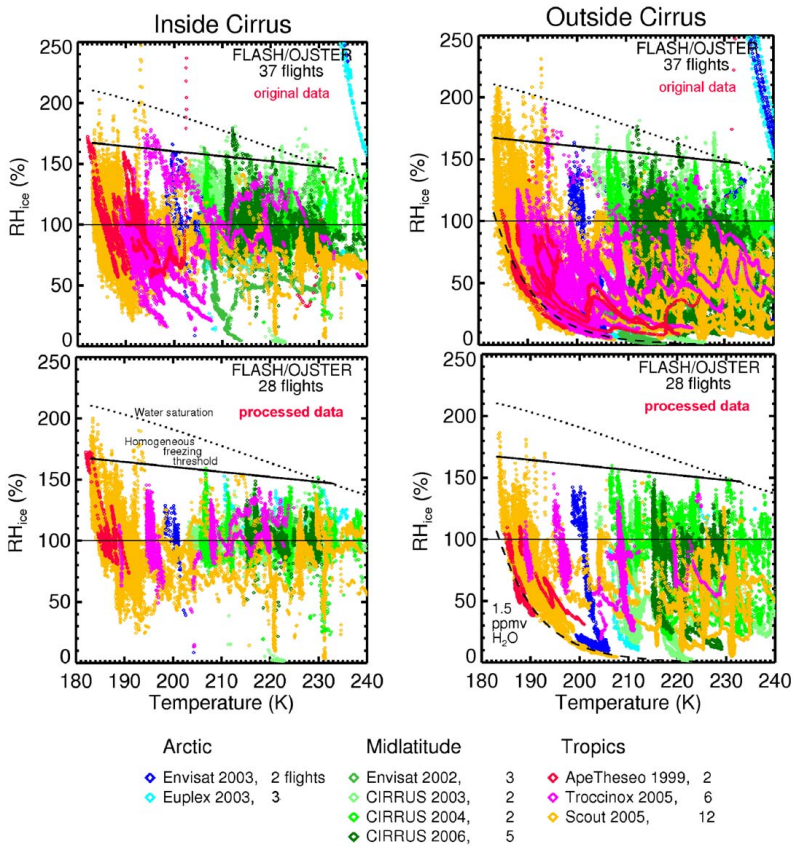

Fig. 3. Field observations of RH_{ice} vs. temperature in- and outside of cirrus. Top panels: original $RH_{ice}(H_2O_{gas,orig})$ measurements of all flights with H_2O_{enh} and $H_2O_{gas,orig}$ measurements; data points represent 15.4/20.8 h in/out-side of cirrus during 37 flights (1 h cruising time represents about 680 km); blueish data points represent Arctic, greenish Mid-latitude and reddish Tropical field campaigns. Bottom panels: Processed $RH_{ice}(H_2O_{gas})$ data; data points represent 9.7/15.9 h in/out-side of cirrus during 28 flights. The black dotted line represents water saturation, the black solid line the homogeneous freezing threshold for liquid solution droplets with 0.5 µm radius (Koop et al., 2000).

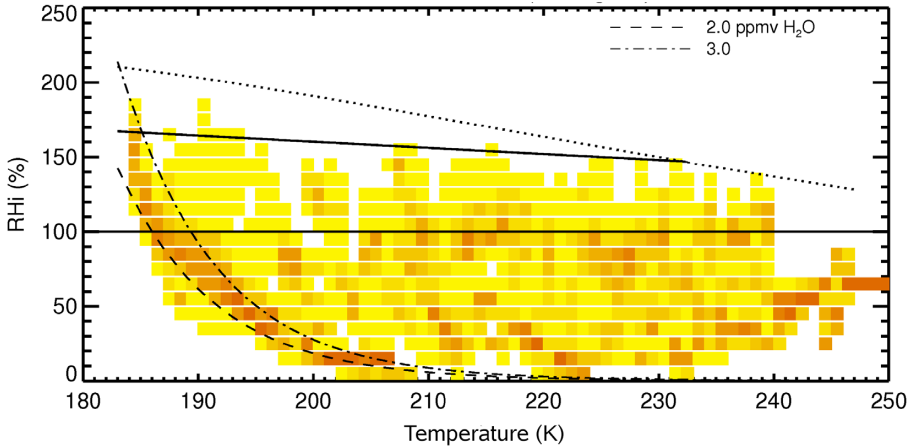

Fig. 4. Same as Fig. 3 (bottom right panel), but as frequencies of occurrence (data are sorted in 1 K temperature bins; solid line: homogeneous freezing threshold, dotted line: water saturation line).

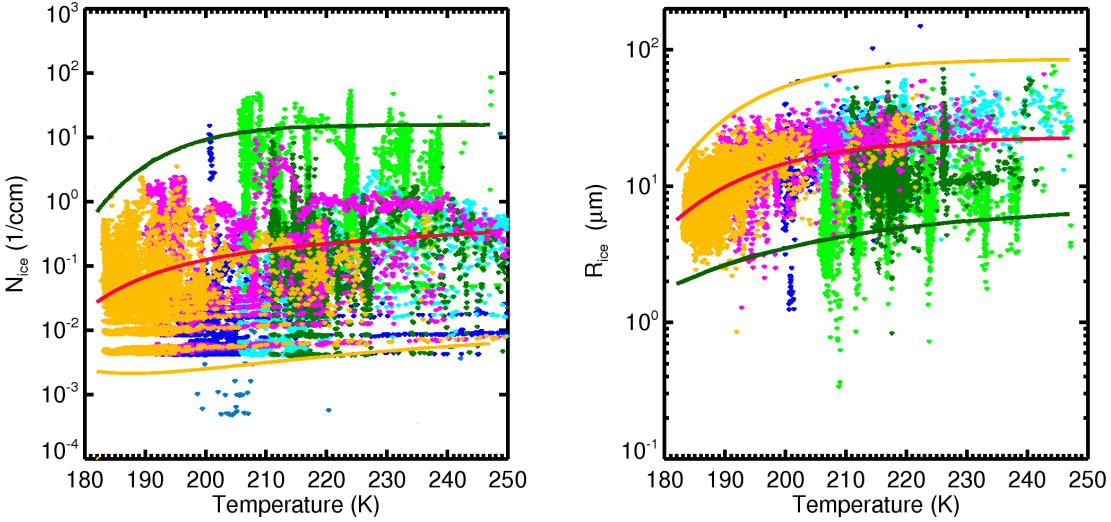

Fig. 5. Ice crystal number N_{ice} and size R_{ice} vs. temperature. Dots: observations from 20 flights (8.5 h inside of cirrus, for colour coding see Fig. 3), lines: minimum, middle and maximum N_{ice} and R_{ice}.

ACPD
8, 21089–21128, 2008

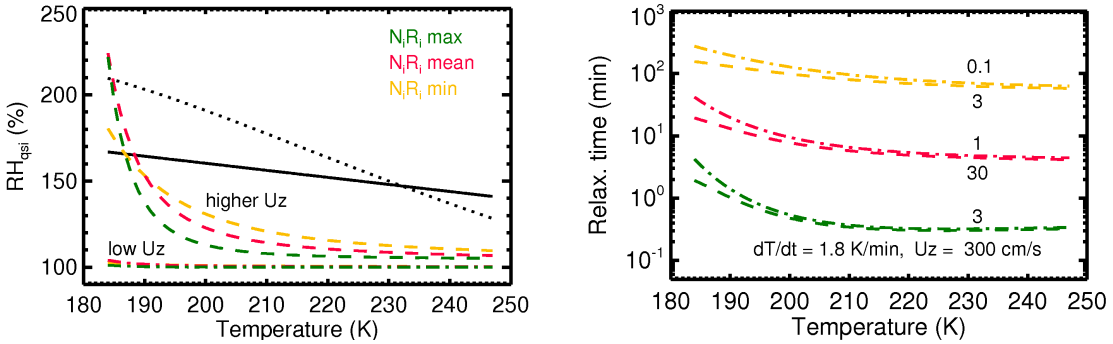

Fig. 6. Quasi steady state RH_{qsi} (left) and relaxation times τ (right) vs. temperature for minimum (yellow), middle (red) and maximum (green) N_iR_i and a high (dashed)/low (dashed-dotted) vertical velocity u_z, respectively ($N_iR_i = N_{ice} \cdot \overline{R_{ice}}$, calculated from the lines in Fig. 5 with $p=p_{mean}(T)$ taken from Schiller et al. (2008), electronic supplement; the black dotted line represents water saturation, the black solid line the homogeneous freezing threshold after Koop et al. (2000); note that the calculations are not for evaporating cirrus, where u_z is negative and RH_{ice} is below saturation); for more information see text.

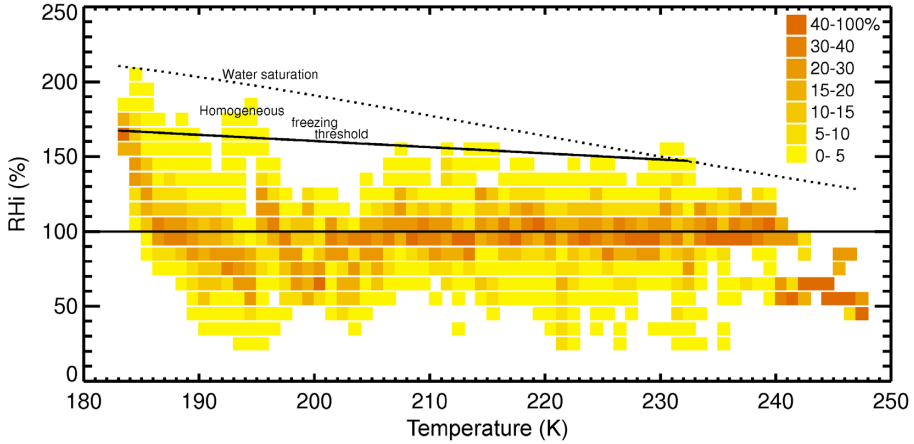

Fig. 7. Frequencies of occurrence of relative humidities over ice RH_{ice} vs. temperature (same data set as in Fig. 3, bottom left, solid line: homogeneous freezing threshold, dotted line: water saturation line; data are sorted in 1 K temperature bins).

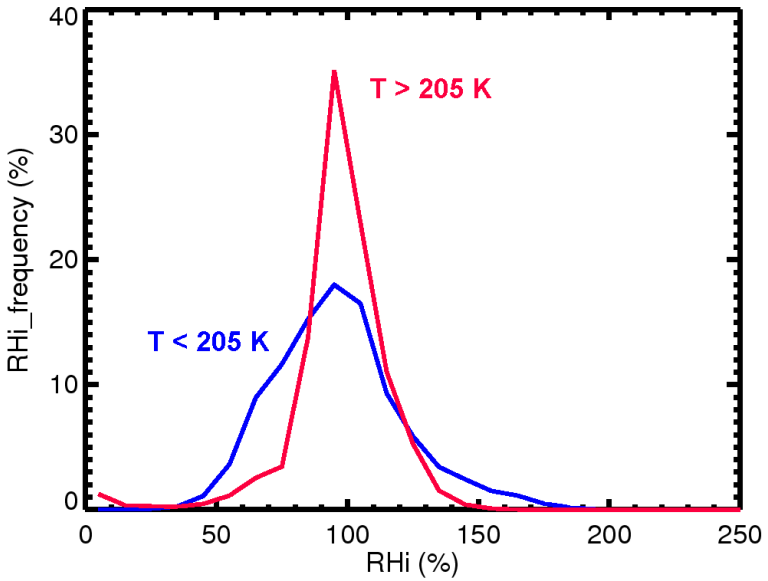

Fig. 8. Frequency distribution of RH_{ice} inside of cirrus for two temperature ranges (T>205 K, red, 5.6 h airborne in-situ observations and T<205 K, blue, 4.1 h; same dataset as Fig. 7, bottom; data are sorted in 5% RH_{ice} bins).

ACPD
8, 21089–21128, 2008

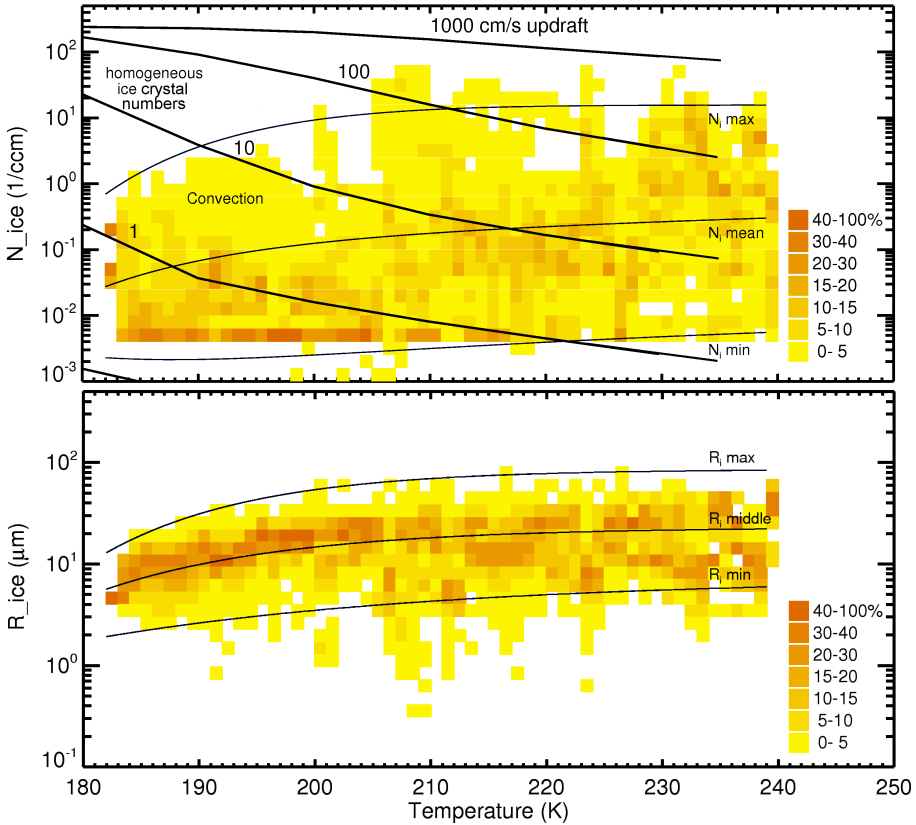

Fig. 9. Frequencies of occurrence of ice crystal numbers N_{ice} (top panel) and sizes R_{ice} (bottom panel) vs. temperature (same dataset as Fig. 5; thin solid lines: minimum, middle and maximum N_{ice} and R_{ice}; thick solid lines in top panel: ice crystal numbers arising for homogeneous freezing at different updraft velocities after Koop et al. (2000) for an aerosol particle number of 300 cm^{-3} and mean pressure; data are sorted in 1 K temperature bins).